Tissue clearing for confocal imaging of native and bio-artificial skeletal muscle tissue

Journal:	*Biotechnic & Histochemistry*
Manuscript ID:	TBIH-2014-0106.R3
Manuscript Type:	Original Paper
Date Submitted by the Author:	03-Feb-2015
Complete List of Authors:	decroix, lieselot; KU Leuven, development and regeneration van muylder, vicky; KU Leuven, development and regeneration desender, linda; KU Leuven, development and regeneration sampaolesi, maurilio; KU Leuven, development and regeneration thorrez, lieven; KU Leuven, development and regeneration
Keywords:	clearing , confocal microscopy, skeletal muscle, bio-artificial muscle, tissue engineering, visualization

Running head:

Clearing muscle for confocal imaging

Correspondence: Lieven Thorrez, Tissue Engineering Lab, Department of Development and Regeneration at Kulak, KU Leuven, E. Sabbelaan 53, 8500 Kortrijk, Belgium. Phone: +32 56 24 62 31, fax: +32 56 24 69 94, e-mail: lieven.thorrez@med.kuleuven.be

Tissue clearing for confocal imaging of native and bio-artificial skeletal muscle

L Decroix[1], V Van Muylder[1], L Desender[1], M Sampaolesi[2], L Thorrez[1,2]

[1]Tissue engineering Lab, Department of Development and Regeneration at Kulak, KU Leuven, E. Sabbelaan 53, 8500 Kortrijk, and [2]Translational Cardiomyology Lab, Department of Development and Regeneration, KU Leuven, O&N4 bus 804, Herestraat 49, 3000 Leuven, Belgium

Abstract

Novel clearing techniques have revolutionized three-dimensional confocal imaging of the brain without the need for physical tissue sectioning. We evaluated three clearing methods, Sca*l*eA2, Clear^{T2}, and 3DISCO for visualizing native and tissue engineered muscle by confocal microscopy. We found that Clear^{T2} treatment improved the depth of visualization of immunohistochemical staining slightly, but did not improve depth of visualization of endogenous green fluorescent protein (GFP). Sca*l*eA2 preserved endogenous GFP signal better and permitted significantly deeper GFP imaging, but it was incompatible with tropomyosin immunohistochemical staining. 3DISCO treatment preserved both endogenous GFP and immunohistochemical staining, and permitted significantly deeper imaging. Clearing time for the 3DISCO procedure is short compared to Sca*l*eA2 and Clear^{T2}. We suggest that 3DISCO is the preferable clearing method for native and tissue engineered skeletal muscle tissue.

Key words: bio-artificial, clearing, confocal microscopy, skeletal muscle, tissue engineering, visualization

Three-dimensional (3D) visualization of tissue is important for studying the morphology and distribution of cells. Confocal microscopy enables optical sectioning of tissues up to 150 µm deep (Miyawaki 2013, Hama et al. 2011). Great progress in 3D imaging has been made during the past decade; images can be obtained deeper in a tissue with increased resolution. Two-photon microscopy enables deeper light penetration and less phototoxicity, because light with a longer wavelength is used, which permits visualization to a depth of 500–800 µm (Miyawaki 2013, Hama et al. 2011). Increased optical path lengths in the sample, however, increases light scattering and limits resolution.

Light sheet microscopy, which differs from conventional wide field and confocal fluorescence microscopy by illumination perpendicular to the direction of observation, has been applied to biology recently to visualize partially transparent samples such as fish embryos (Huisken et al. 2004). Most biological tissues, however, are relatively opaque, which prevents high resolution imaging of thick specimens. Moreover, the different compositions of the cell membrane (lipid) and intra- and extracellular fluids create a refractive index interface that scatters light. Consequently, methods have been developed to clear biological samples. Optical light scattering can be reduced by optical clearing, which renders tissue specimens transparent, to achieve refractive uniformity throughout the

specimen. Optical clearing is achieved by incubating the fixed sample with a clearing agent. Dehydration of the sample is required before clearing with hydrophobic clearing agents. The clearing agent, which has a high refractive index similar to the refractive index of lipids, is used to replace the aqueous intra- and extracellular fluids. This reduces light scattering between the cell membrane (lipid) and the intra- and extracellular fluid and renders the tissue more transparent (Sakhalkar et al. 2007).

Although tissue clearing techniques were pioneered a century ago (Spalteholz 1914), their use has become widely appreciated only recently. Clearing first became critical for modern imaging methods for optical projection tomography, which enabled visualization of whole mouse embryos (Sharpe et al. 2002). These investigators used a 2:1 mixture of benzylbenzoate:benzyl alcohol (BABB) following dehydration with ethanol and hexane. This protocol is not fully compatible with fluorescence, however, and other clearing agents were developed to preserve better the fluorescent signals from labeled cells.

New tissue clearing techniques have been used mainly for embryological and neural research (Becker et al. 2012, Chung et al. 2013, Hama et al. 2011, Kuwajima et al. 2013, Sakhalkar et al. 2007). The efficacy of these agents for adult muscle or tissue engineered muscle, however, has not been demonstrated.

Tissues possess different extracellular matrix (ECM) compositions, microvasculature and cell types, all of which produce different light scattering effects. These structures affect the extent to which the tissue is rendered transparent by clearing.

We evaluated the efficacy of three recently described clearing methods: Sca*l*eA2 (Hama et al. 2011), Clear^{T2} (Kuwajima et al. 2013) and 3DISCO (Ertürk et al. 2012). These methods were used originally for imaging mouse brains and ostensibly maintained fluorescence. We evaluated depth of visualization by confocal imaging in green fluorescent protein (GFP)-expressing mouse skeletal muscle before and after clearing. We then assessed the suitability of these clearing techniques for visualizing myofiber organization and endothelial cell network formation in tissue engineered bio-artificial muscle (BAM) constructs.

BAMs can be created in vitro by culturing and differentiation of adult myogenic progenitor cells in hydrogels, such as fibrin or collagen (Thorrez et al. 2006, Vandenburgh et al. 2008). BAMs are composed of aligned multinucleated myofibers, which generate tension and can be stimulated electrically to generate active force (Powell et al. 2002, Vandenburgh et al. 2008). The BAM system is a well-defined model for studying in vitro differentiation of myogenic progenitor cells, myofiber formation and the effect of drugs on muscle force generation

(Vandenburgh et al. 2008). BAMs enable characterization of myofiber properties including alignment, shape and fusion index, as well as behavior, e.g., cellular distribution and differentiation of other cell types in co-culture. Unlike muscle in vivo, current state-of-the-art BAMs lack innervation, fat tissue, organized connective tissue and vascularization.

To study vasculogenesis using the BAM model, we traced the distribution and organization of GFP-labeled human umbilical vein endothelial cells (HUVECs), co-cultured in 3D, throughout the BAM. Light scattering and refraction, however, limited the depth of visualization, which prevented 3D imaging of the entire BAM.

Material and methods

All animal experiments were carried out in compliance with the Ethical Guidelines of KU Leuven.

Cell culture

HUVECs that constitutively express GFP (Angio-proteomie, Boston, MA) were cultured in T25 culture flasks coated with gelatin (Millipore, Billerica, MA) in endothelial growth medium (EGM-2 using a bullet kit, composed of basal medium and supplements, Lonza, Basel, Switzerland). GFP-HUVECs were divided at 90% confluence and used for our experiment at passage 7. Human myoblasts isolated from a healthy 52-year-old male (gift from Dr. H. Vandenburgh) were cultured in skeletal muscle growth medium (SkGM; Lonza) supplemented with 15% fetal bovine serum (FBS; Life Technologies, Carlsbad, CA). Myoblasts were divided at 60−70% confluence and used in experiments at about 20 doublings.

Tissue engineering

BAMs were constructed in custom molds with a total casting volume of 1 ml. One million cells were mixed with either fibrin or collagen based hydrogels. Cells used in the BAMs were a mixture of 7 x 10^5 human myoblasts and 3 x 10^5 GFP-HUVECs.

For fibrin BAMs, cells were mixed in a fibrin hydrogel (1 mg/ml) and for collagen BAMs the hydrogel was composed of 1 mg/ml rat tail collagen with 13% matrigel (BD Biosciences, San Jose, CA) as described earlier (Thorrez et al. 2008). The constructs were kept in culture for 7 days in EGM-2 medium to allow myoblast fusion and differentiation to myofibers, and endothelial network formation.

Whole mount fluorescent staining and confocal microscopy

BAMs were washed three times in phosphate-buffered saline (PBS; Invitrogen, Carlsbad, CA), then removed from the molds. They then were fixed in 4% formaldehyde (Merck, Darmstadt, Germany) for 1 h and stored at 4° C in PBS. Samples were fixed a second time in methanol at -20° C for 20 min, then washed three times in PBS for 15 min each time. Samples were permeabilized and nonspecific binding was blocked by incubation at room temperature for 1 h in blocking buffer containing 1% bovine serum albumin (BSA) (Sigma-Aldrich, St. Louis, MO) and 0.2% Triton-X-100 (Sigma-Aldrich) in PBS. Subsequently, BAMs were incubated overnight at 4° C with a primary anti-tropomyosin antibody (T9283; Sigma) 1:100 in blocking buffer. BAMs then were washed three times with PBS for 15 min each time and incubated with a goat anti-mouse secondary antibody (Alexa Fluor 568; Invitrogen) for 30 min in the dark. BAMs were washed

three times with PBS for 15 min each time and incubated in DAPI (Invitrogen) (1:10000 in PBS) for 1 h. BAMs were stored in PBS in the dark, viewed by confocal microscopy within 48 h, then cleared. In some cases, a second fluorescence staining was performed after the clearing procedure as described above.

Adult skeletal muscle

Skeletal muscle (quadriceps and gastrocnemius) was obtained from the hind limbs of a female beta β-actin-GFP mouse model (kindly donated by Dr. P. Carmeliet). Skeletal muscle was rinsed three times in PBS and fixed overnight in 4% formaldehyde.

Clearing

After fixation, mouse skeletal muscle tissue and BAMs were subjected to one of the following clearing agents: Clear^{T2} (Kuwajima et al. 2013), ScaleA2 (Hama et al. 2011) or 3DISCO (Ertürk et al. 2012).

For clearing with Clear^{T2}, a 20% polyethylene glycol (PEG) solution was prepared by stirring powdered PEG 4000 MW (Sigma-Aldrich) in water at 37° C for 30 min. Skeletal muscle and BAMs first were immersed for 1 h at room

temperature in 25% formamide (Sigma-Aldrich):10% PEG solution followed by incubation for 12 h in 50% formamide:20% PEG solution.

For clearing with Sca*l*eA2, mouse skeletal muscle tissue and BAMs were incubated for 2 weeks in Sca*l*eA2 solution, which is composed of 4 M urea (Sigma-Aldrich), 10% (w/v) glycerol (Acros, Geel, Belgium) and 0.1% (w/v) Triton-X-100 (Sigma-Aldrich).

For 3DISCO clearing, skeletal muscle and BAMs were treated as described earlier (Ertürk et al. 2012). Briefly, tissues were placed in small glass bottles and dehydrated with increasing concentrations of tetrahydrofuran (THF) in MilliQ (Millipore) filtered water. Glass vials containing 50, 70, 80 and 100% THF were placed on a rotating wheel in the dark. Each dehydration step was a single incubation for 30 min, except for the last step, which was repeated three times. After dehydration, clearing was performed with dibenzyl ether (DBE) for 1 h (Becker et al. 2012). After clearing, mouse skeletal muscle tissues and BAMs were imaged macroscopically (Sony DSCWX60W, Tokyo, Japan) to document changes in transparency, then viewed by confocal microscopy.

Confocal imaging

Imaging was performed using an LSM710 confocal microscope (Zeiss, Oberkochen, Germany and Zen software (Zeiss). All images were acquired using a 25 x objective, NA = 0.55, and working distance of 26 mm.

Statistics

Data are presented as means ± standard deviations and statistical analyses were performed using GraphPad Prism; n represents the number of images that were analyzed. One-way ANOVA was used for testing multiple groups. To examine tissue shrinkage or expansion, we measured tissues along the x, y and z axes and calculated the ratios before and after clearing, which were compared to 1 (H_0 = no length change) by a one sample t-test. We used a confidence level of $p \leq 0.05$.

Results

Clearing mouse skeletal muscle

Adult mouse skeletal muscle tissue that constitutively expressed GFP under control of a β-actin promoter was used to test the effect of different clearing agents on confocal imaging depth. Muscle tissue was fixed overnight in 4% formaldehyde, imaged by confocal microscopy, then subjected to clearing agents Sca*l*eA2 (Hama et al. 2011), Clear^{T2} (Kuwajima et al. 2013) or 3DISCO (Ertürk et al. 2012). Clearing with Sca*l*eA2 required 2 weeks compared to 13 h with Clear^{T2} and 4 h with 3DISCO. After clearing with Sca*l*eA2, mouse skeletal muscle appeared slightly more transparent than uncleared fixed tissue, but Clear^{T2} treatment did not cause macroscopically observable improvement in tissue transparency. Clearing with 3DISCO resulted in remarkably transparent tissue (Fig. 1). Muscle treated with 3DISCO hardened the tissue, by contrast to the other clearing procedures.

The GFP signal could be detected to a depth of 162.3 ± 29.5 µm (n = 30) in uncleared muscle tissue. Spatial resolution that permitted identification of separate myofibers, however, could be obtained only to a depth of 74.5 ± 22.2 µm (n = 20) (Fig. 2). After Clear^{T2} treatment, the GFP imaging depth was 179.2 ±

40.2 µm (n = 18), which was not significantly different from untreated muscle tissue (Figs. 2, 3A). In addition, spatial resolution was slightly better than, but not significantly different from untreated muscle; identification of separate myofibers extended to a depth of 83.4 ± 25.0 µm (n = 16).

The GFP signal in muscle tissue cleared with Sca*l*eA2 was detected to a depth of 313.3 ± 41.4 µm (n = 15), which was significantly deeper than for untreated tissue (Figs. 2, 3A) ($p < 0.001$). Owing to improved transparency and enhanced light penetration, resolution improved significantly compared to untreated tissue to allow identification of separate myofibers at a maximum depth of 145.8 ± 56.1 µm (n = 18) ($p < 0.001$).

3DISCO clearing of GFP muscle tissue enabled detection of GFP signal to a depth of 400.8 ± 30.6 µm (n = 18), which was significantly deeper than for untreated tissue ($p < 0.001$) (Figs. 2, 3A). Separate myofibers could be distinguished with adequate resolution five times deeper than in uncleared tissue and more than twice as deep as Sca*l*eA2 cleared specimens (372.1 ± 46.2 µm, n = 16). Figure 3A shows image depth quantitatively following Clear^{T2}, Sca*l*eA2 or 3DISCO treatments versus uncleared tissue.

We investigated possible muscle tissue shrinkage or expansion due to clearing and found 2.8 ± 8.6% (n = 12) and 19.9 ± 15.6% (n = 9) linear shrinkage

after Clear^{T2} or 3DISCO treatment, respectively, and 4.4 ± 20.5 % (n = 8) linear expansion after Sca*l*eA2. Only 3DISCO treatment caused significant shrinkage compared to untreated tissue ($p < 0.01$).

Clearing BAM

BAMs differ from muscle in vivo; they lack innervation and vascularization, and are composed of extracellular matrix that lacks organized connective tissue. Therefore, we also tested whether clearing agents could affect the transparency and depth of visualization for BAMs.

In uncleared fibrin BAMs, GFP-HUVECs were visible to a depth of 180.8 ± 18.37 µm (n = 20) with sufficient resolution to distinguish individual cells. In uncleared collagen BAMs, GFP-HUVECs were visible to a depth of 157.5 ± 18.0 µm (n = 10), which was not significantly different from fibrin BAMs.

Collagen BAMs did not appear more transparent than untreated BAMs after clearing with either Sca*l*eA2 (2 weeks) or Clear^{T2} for 13 h, but they had a transparent and glazed appearance after 3DISCO clearing (Fig. 4). Fibrin BAMs did not appear more transparent after Clear^{T2} treatment, but Sca*l*eA2 and 3DISCO treatment produced obvious clearing (Fig. 4). Like native muscle tissue, 3DISCO

treatment hardened the BAMs, whereas ScaleA2 treatment produced softer, almost slimy tissue, which made the BAM structure more difficult to handle.

After clearing fibrin BAMs with Clear^{T2}, the mean depth of visualization of GFP was 133.9 ± 56.7 µm (n = 14), which was significantly less than the uncleared BAMs (Fig. 3B). Representative images of Clear^{T2} treated BAMs are shown in Fig. 5A. After Sca*l*eA2 clearing of fibrin BAMs, the mean depth of visualization of the endogenous GFP signal of HUVECs was increased significantly to 290.0 ± 24.4 µm (n = 15) compared to 180.8 ± 18.4 µm (n = 20) for uncleared BAMs ($p < 0.001$) (Fig. 4). 3DISCO clearing of fibrin BAMs enabled visualization of GFP signals to a mean depth of 293.0 ± 34.4 µm (n = 10), which was significantly deeper than for uncleared BAMs (Figs. 4, 5A). In addition, 3DISCO clearing of collagen BAMs produced a significant increase in the mean depth of GFP signal detection to 500 ± 33.0 µm (n = 5) compared to untreated BAMs (157.5 ± 18.0 µm) (n = 10). An example of increased imaging depth in fibrin BAMs is shown in Fig. 5A as increased depth along the z axis. Note that the imaging depth for the fibrin BAMs included the full thickness of the BAM.

Immunohistochemical staining for tropomyosin, a marker for myofibers, was performed on fixed tissue prior to clearing. This staining clearly labeled myofibers red (Alexa 568) and myofiber alignment could be assessed to a depth

of 142.3 ± 23.4 µm (n = 30) (Fig. 5B). Red fluorescence from labeled myofibers was undetectable after clearing with Sca*l*eA2. Therefore, immunohistochemical staining for tropomyosin was performed again after clearing to test whether the antibody could still recognize tropomyosin. Unfortunately, immunohistochemical staining after clearing with Sca*l*eA2 was unsuccessful.

By contrast to clearing with Sca*l*eA2, clearing in Clear^{T2} preserved tropomyosin immunohistochemical staining in fibrin BAMs (Fig. 5B). Despite a weaker signal, clearing of fibrin BAMs using Clear^{T2} resulted in significantly increased visualization of immunohistochemically stained myofibers to a depth of 166.0 ± 19.1 µm (n = 10) compared to uncleared tissue ($p < 0.05$). 3DISCO clearing of fibrin BAMs also preserved immunohistochemical staining and permitted visualization of the stained myofibers to a depth of 293.0 ± 34.4 µm (n = 10) (Fig. 5B), a significant increase compared to uncleared tissue ($p < 0.001$).

Discussion

Three-dimensional visualization of tissues has improved dramatically owing to novel microscopy techniques and improved tissue processing and staining methods. The depth of visualization of tissue remains limited due to scattering and refraction of light as it penetrates the tissue. Two-photon microscopy based on a femtosecond laser enables deeper photon penetration and less cytotoxicity, but with lower resolution.

Optical clearing is an emerging technology for reducing light scattering by increasing tissue transparency, which increases depth of imaging. Great improvement in clearing thick tissue has been demonstrated for brain (Chung et al. 2013, Hama et al. 2011, Kuwajima et al. 2013). Sca*l*eA2 has been used to study the vascular niche for neural stem cells (Hama et al. 2011), whereas Clear^{T2} has been used to improve imaging of axonal projections (Kuwajima et al. 2013). Tissues such as brain, spinal cord, immunity organs and tumors were cleared efficiently using 3DISCO (Ertürk et al. 2012). Because these clearing methods might be useful for other tissues, we investigated their potential for muscle research and muscle tissue engineering where 3D imaging is important for investigating cell behavior including survival, proliferation, migration and differentiation.

Without clearing, confocal imaging of endogenous GFP in native mouse muscle could be detected 162.3 ± 29.5 µm deep in the tissue; however, good resolution was obtained only to 74.5 ± 22.2 µm, the thickness of 1−2 myofibers. Clearing the muscle with Clear^{T2} did not significantly increase the depth of visualization. By contrast, after Sca*l*eA2 clearing, the GFP signal could be detected to 313.3 ± 41.4 µm with good resolution to 145.8 ± 56.1 µm deep, an increase in depth of 50%. Compared to uncleared tissue, 3DISCO clearing produced a 250% increase in depth of GFP visualization (400.8 ± 30.6 µm) with a 500% increase (372.1 ± 46.2 µm) in depth of optimal resolution. Macroscopic observations indicated that Clear^{T2} did not improve tissue transparency, whereas Sca*l*eA2 clearly improved transparency and 3DISCO produced a glass-like consistency.

Neither Sca*l*eA2 nor Clear^{T2} significantly altered the size of the muscle specimens, while 3DISCO caused significant shrinkage of the tissue. To the contrary, Kuwajima et al. (2013) reported that Sca*l*eA2 clearing of brain caused a 1.25-fold linear expansion. Differences in shrinkage, as well as differences in efficiency of the clearing procedures likely can be attributed to the different composition of brain tissue compared to skeletal muscle.

Mature skeletal muscle differs from bio-artificial muscle in vascularization, innervation and composition of extracellular matrix. The composition of the

extracellular matrix affects tissue opacity and therefore also the result of optical clearing. We created BAMs with a fibrin extracellular matrix and a type I collagen extracellular matrix. For BAMs with a collagen extracellular matrix, clearing with Sca*l*eA2 or Clear^{T2} did not increase the transparency of the tissue. By contrast, 3DISCO produced maximal transparency for the collagen and fibrin BAMs.

Sca*l*eA2 significantly increased the depth of visualization of endogenous GFP in fibrin BAMs from 180.8 ± 18.4 µm (uncleared) to 290.0 ± 24.4 µm, a 60% increase. Sca*l*eA2 caused disruption of the fluorescent signal of immunohistochemical staining for tropomyosin, however, and the tissue could not be re-stained after clearing. Our observations differ from those of Hama et al. (2011), who reported at least some successful immunohistochemical staining in mouse brain after Sca*l*eA2 clearing. Consistent with our observations, however, Kuwajima et al. (2013) reported that Sca*l*eA2 and BABB disrupt the fluorescent signal of conventional lipophilic carbocyanine dyes and certain fluorescent tracers. Another disadvantage of Sca*l*eA2 compared to Clear^{T2} and 3DISCO is the time required for clearing: 2 weeks versus < 1 day.

Clear^{T2} treatment did not increase the depth of visualization of endogenous GFP in fibrin BAMs and it reduced the endogenous GFP signal. On the other hand, Clear^{T2} was compatible with immunohistochemical staining and enabled 17%

deeper imaging of the stained myofibers. Our observation that Clear^{T2} treatment increased the depth of visualization of immunohistochemical staining is consistent with a report for brain tissue (Kuwajima et al. 2013).

3DISCO clearing not only produced a 62% increase in the depth of visualization of endogenous GFP signals, it also preserved immunohistochemical staining and caused a two-fold increase in depth of visualization of stained myofibers. Because 3DISCO treatment hardens tissue, the original cylindrical shape of the bio-artificial muscles is retained, by contrast to Clear^{T2} and Sca*l*eA2, which caused the tissue to soften and flatten when placed on a glass slide. We demonstrated that bio-artificial muscle can be visualized throughout its diameter after 3DISCO clearing (Fig. 5A, B).

We found that for both native and tissue engineered muscle, Clear^{T2} treatment does not improve depth of visualization of endogenous GFP. Although Clear^{T2} preserves immunohistochemical staining, it cannot be recommended as a clearing agent for native and engineered muscle tissue. Sca*l*eA2 is a good clearing agent that preserves endogenous GFP and permits deep imaging of GFP. The disadvantages of Sca*l*eA2 include the requirement for a long incubation time (2 weeks) and its incompatibility with immunohistochemical staining. For both native and tissue engineered muscle, we demonstrated that 3DISCO treatment is

rapid and permits deep imaging of both endogenous GFP and immunohistochemical staining. We suggest that 3DISCO is the clearing method of choice for native and tissue engineered muscle.

Acknowledgments

The authors thank Sebastian Munck for expert advice regarding microscopy techniques, Petra D'hooge for technical assistance with confocal microscopy, Sigrid Vanryckeghem for administrative support, Kristel Eggermont for tissue isolation and Dr. Melanie Gerard for critical reading of the manuscript. We also thank Dr. Herman Vandenburgh for kind donation of human myoblasts and advice and Dr. Peter Carmeliet for kind donation of GFP mouse muscle. This work was funded by the Research Fund KU Leuven (CREA/12/034). LT is a Postdoctoral Fellow of the Research Foundation-Flanders (FWO).

Declaration of interest: The authors report no conflicts of interest. The authors alone are responsible for the content and writing of this paper.

References

Becker K, Jährling N, Saghafi S, Weiler R, Dodt HU (2012) Chemical clearing and dehydration of GFP expressing mouse brains. *PLoS One* 7: e33916.

Chung K, Wallace J, Kim SY, Kalyanasundaram S, Andalman AS, Davidson TJ, Mirzabekov JJ, Zalocusky K, Mattis J, Denisin AK (2013) Structural and molecular interrogation of intact biological systems. *Nature* 497: 332–337.

Ertürk A, Becker K, Jährling N, Mauch C, Hojer C, Egen J, Hellal F, Bradke F, Sheng M, Dodt H (2012) Three-dimensional imaging of solvent-cleared organs using 3DISCO. *Nat. Protoc.* 7: 1983–1995.

Hama H, Kurokawa H, Kawano H, Ando R, Shimogori T, Noda H, Fukami K, Sakaue-Sawano A, Miyawaki A (2011) Scale: a chemical approach for fluorescence imaging and reconstruction of transparent mouse brain. *Nat. Neurosci.* 14: 1481–1488.

Huisken J, Swoger J, Del Bene F, Wittbrodt J, Stelzer EHK (2004) Optical sectioning deep inside live embryos by selective plane illumination microscopy. *Science* 305: 1007–1009.

Kuwajima T, Sitko A , Bhansali P, Jurgens C, Guido W, Mason C (2013) ClearT: a detergent- and solvent-free clearing method for neuronal and non-neuronal tissue. *Development* 140: 1364–1368.

Miyawaki A (2013) Fluorescence imaging in the last two decades. *Microscopy* 62: 63–68.

Powell C, Smiley BL, Mills J, Vandenburgh HH (2002) Mechanical stimulation improves tissue-engineered human skeletal muscle. *Am. J. Physiol. Cell Physiol.* 283: 1557–1565.

Sakhalkar HS, Dewhirst M, Oliver T, Cao Y, Oldham M (2007) Functional imaging in bulk tissue specimens using optical emission tomography: fluorescence preservation during optical clearing. *Phys. Med. Biol.* 52: 2035–2054.

Sharpe J, Ahlgren U, Perry P, Hill B, Ross A, Hecksher-Sørensen J, Baldock R, Davidson D (2002) Optical projection tomography as a tool for 3D microscopy and gene expression studies. *Science* 296: 541–545.

Spalteholz W (1914) *Über das Durchsichtigmachen von menschlichen und tierischen Präparaten und seine theoretischen Bedingungen, nebst Anhang: Über Knochenfärbung.* S Hirzel, Leipzig.

Thorrez L, Vandenburgh H, Callewaert N, Mertens N, Shansky J, Wang L, Arnout J, Collen D, Chuah M, Vandendriessche T (2006) Angiogenesis enhances factor IX delivery and persistence from retrievable human bioengineered muscle implants. *Mol. Ther*. 14: 442–451.

Thorrez L, Shansky J, Wang L, Fast L, VandenDriessche T, Chuah M, Mooney D, Vandenburgh H (2008) Growth, differentiation, transplantation and survival of human skeletal myofibers on biodegradable scaffolds. *Biomaterials* 29: 75–84.

Vandenburgh H, Shansky J, Benesch-Lee F, Barbata V, Reid J, Thorrez L, Valentini R, Crawford G (2008) Drug-screening platform based on the contractility of tissue-engineered muscle. *Muscle Nerve* 37: 438–447.

Fig. 1. Transparency of mouse skeletal muscle before and after clearing with Clear^{T2}, Sca*l*eA2 and 3DISCO. Scale bar = 1 cm.

Fig. 2. Depth of GFP detection in mouse GFP-expressing skeletal muscle tissue. Confocal imaging of mouse GFP-expressing skeletal muscle tissue before and after clearing with Clear^{T2}, Sca*l*eA2 and 3DISCO. Three-dimensional reconstructions of image stacks. Note the differences of imaging depth on the z axis.

Fig. 3. Quantitative representation of GFP imaging depth in mouse GFP-expressing skeletal muscle tissue and fibrin BAMs containing GFP-expressing HUVECs. A) Box plot representing depth of GFP signal in uncleared, Clear^{T2}, Sca*l*eA2 and 3DISCO cleared mouse GFP-expressing skeletal muscle tissue. B) Box plot representing depth of GFP signal in uncleared, Clear^{T2}, Sca*l*eA2 and 3DISCO cleared fibrin BAMs containing 3 x 10^5 GFP-expressing HUVECs and 7 x 10^5 myoblasts. $^{**}p < 0.01$, $^{***}p < 0.001$.

Fig. 4. Transparency of bio-artificial muscle before and after clearing. First column) BAMs constructed in a collagen ECM without clearing and after clearing with Clear^{T2}, Sca*l*eA2 and 3DISCO. Second column) BAMs constructed in a fibrin ECM, without clearing and cleared in Clear^{T2}, Sca*l*eA2 and 3DISCO. Scale bar = 1 cm.

Fig. 5. Three-dimensional reconstruction of confocal images of fibrin bio-artificial muscles. A) GFP signals in bio-artificial muscles containing GFP-expressing HUVECs are shown before and after clearing with Clear^{T2}, ScaleA2 and 3DISCO. B) Immunohistochemical staining of tropomyosin (muscle-specific marker; red) and endogenous GFP fluorescence (green) in fibrin BAMs containing GFP-HUVECs and myoblasts before and after clearing with Clear^{T2} and 3DISCO.

Figure 1

75x36mm (300 x 300 DPI)

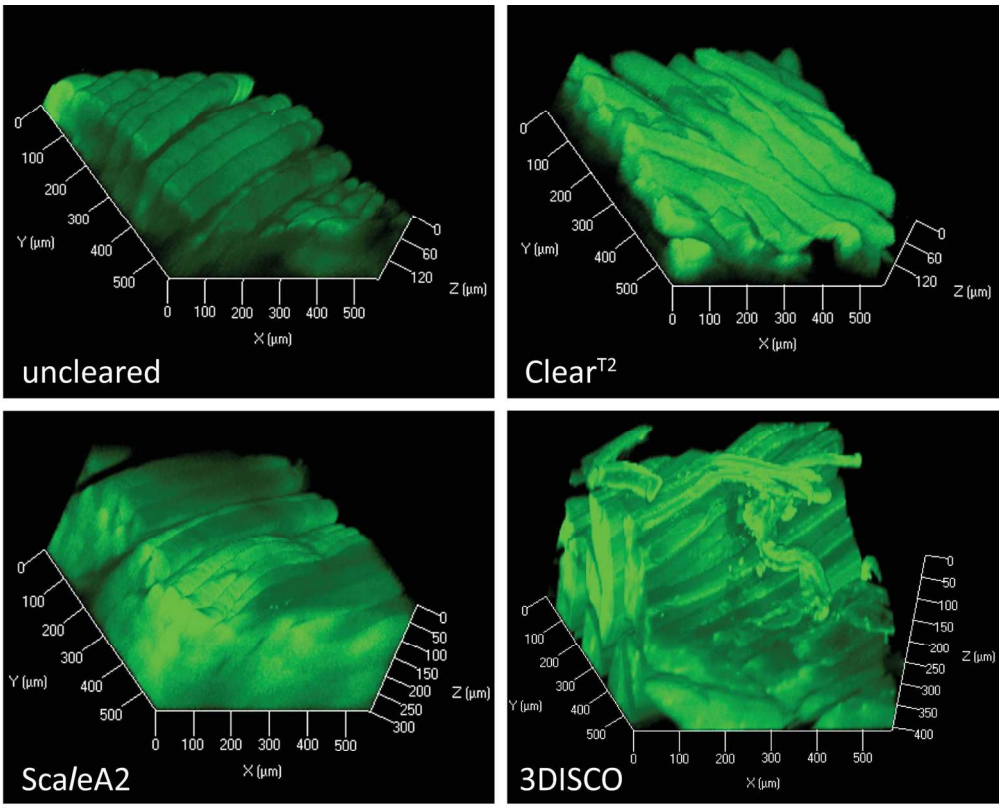

Figure 2

156x133mm (300 x 300 DPI)

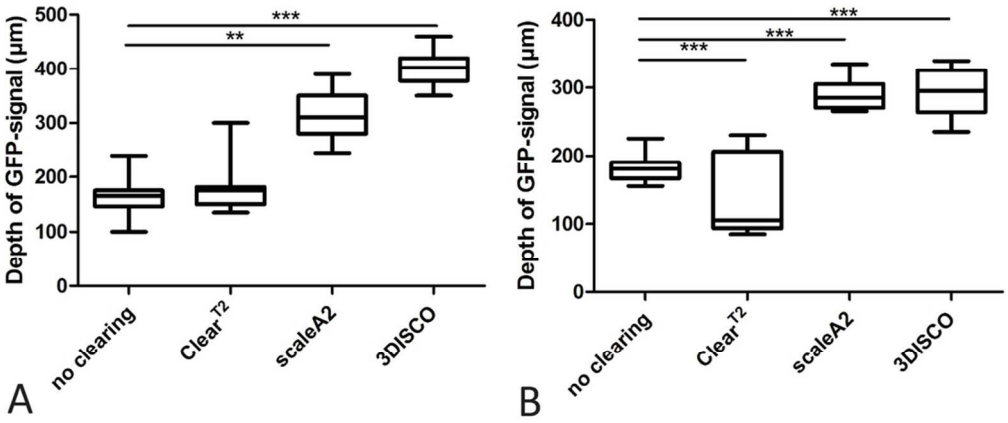

Figure 3

92x60mm (300 x 300 DPI)

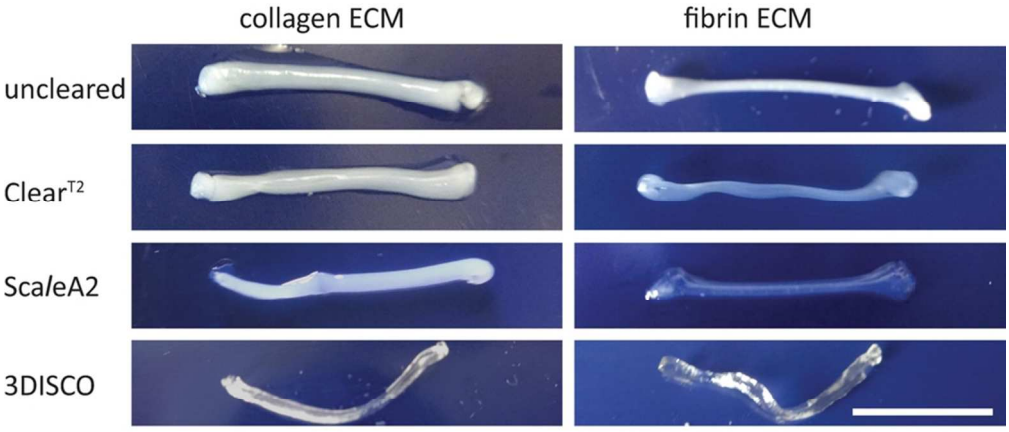

Figure 4

80x39mm (300 x 300 DPI)

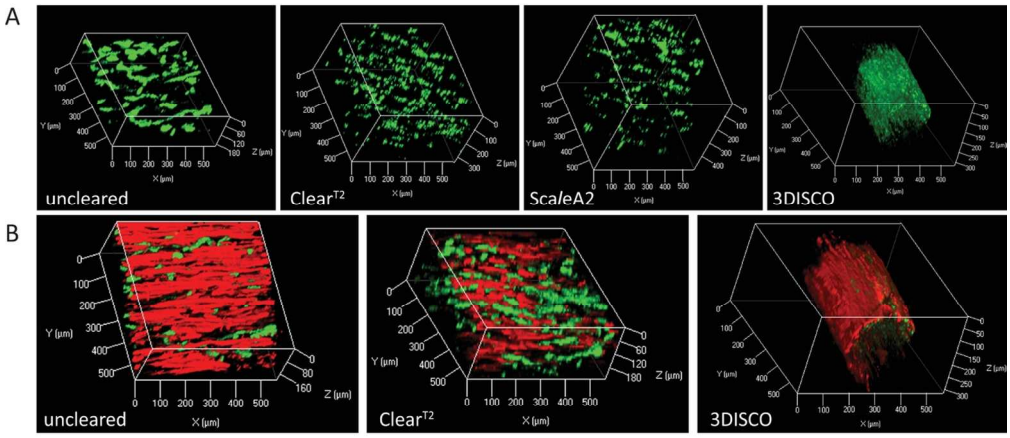

Figure 5

119x60mm (300 x 300 DPI)